

Monitoring Vital Signs Using Millimeter Wave

Zhicheng Yang, Parth H. Pathak, Yunze Zeng, Xixi Liran, Prasant Mohapatra
University of California, Davis, CA 95616, USA
Email: {zcyang, phpathak, zeng, xliran, pmohapatra}@ucdavis.edu

ABSTRACT

Continuous monitoring of human's breathing and heart rates is useful in maintaining better health and early detection of many health issues. Designing a technique that can enable contactless and ubiquitous vital sign monitoring is a challenging research problem. This paper presents mmVital, a system that uses 60 GHz millimeter wave (mmWave) signals for vital sign monitoring. We show that the mmWave signals can be directed to human's body and the RSS of the reflections can be analyzed for accurate estimation of breathing and heart rates. We show how the directional beams of mmWave can be used to monitor multiple humans in an indoor space concurrently. mmVital relies on a novel human finding procedure where a human can be located within a room by reflection loss based object/human classification. We evaluate mmVital using a 60 GHz testbed in home and office environment and show that it provides the mean estimation error of 0.43 Bpm (breathing rate) and 2.15 bpm (heart rate). Also, it can locate the human subject with 98.4% accuracy within 100 ms of dwell time on reflection. We also demonstrate that mmVital is effective in monitoring multiple people in parallel and even behind the wall.

CCS Concepts

•**Human-centered computing** → **Ubiquitous and mobile computing systems and tools**; •**Applied computing** → *Health care information systems*; •**Hardware** → *Signal processing systems*;

Keywords

Millimeter Wave, 60 GHz, Vital Signs, Human Tracking, Signal Reflection and Blockage, Healthcare, Smart Home

1. INTRODUCTION

Monitoring vital signs such as breathing rate and heart rate can provide crucial insights in human's well-being and can detect a wide range of medical problems. Continuous and ubiquitous monitoring of person's vital signs is a challenging problem and the current solutions require the person to wear dedicated devices. Wearable devices such as wrist-worn heart rate monitors, chest straps

for breathing rate detection are required to be connected to the human's body at all times (even during sleep), making them a less convenient alternative. This has motivated the design of contactless solutions for vital sign monitoring where person's smartphone or other nearby communication infrastructure (e.g. WiFi) can be leveraged for the purpose.

In the RF-based vital sign monitoring solutions proposed in [5, 18, 22, 24], WiFi signal reflected from the human body is used to estimate the breathing and heart rates. Although these papers have solved important challenges in designing contactless vital sign monitoring, they have many practical limitations. Due to the omnidirectional propagation commonly used in 2.4/5 GHz WiFi, signal can be reflected from multiple humans in an indoor space. This makes it difficult to distill the vital signs of multiple humans from the reflected signal. Due to this reason, the majority of the WiFi-based vital sign monitoring research assumes there is only a single human subject in the range of WiFi endpoints or if there are multiple humans in the range, their vital signs are sufficiently different from each other. However, in most practical scenarios, there are more than one humans in indoor spaces like homes, offices, hospitals and the vital signs of individuals can vary substantially in a short time. The WiFi signal can also reflect from many indoor objects, and complex signal processing is necessary to extract the human reflected signal in multi-path rich indoor environment. This makes it difficult to determine the tiny motion of heartbeats from the reflected signal and hence [5, 22, 24] are primarily limited to measuring only the breathing rate.

This paper investigates the use of 60 GHz millimeter-wave signal (mmWave) for ubiquitous and non-invasive vital sign monitoring. The 60 GHz mmWave frequency band provides over 7 GHz (57 - 64 GHz) of unlicensed spectrum. With development of IEEE 802.11ad [15], the mmWave band is shown to enable high-speed (up to 7 Gbps) indoor wireless local/personal area networks. Its suitability for applications such as point-to-point video streaming has resulted in rapid commercialization with development of WiFi+60 GHz wireless access points [2], smartphone chipsets etc. With this momentum, the 60 GHz mmWave is likely to be an omni-present technology of indoor WLANs/WPANs in homes and offices in the coming years. We demonstrate that the 60 GHz mmWave signal can provide highly accurate and reliable vital sign monitoring. Due to high attenuation loss of 60 GHz signal, directional beamforming is employed using phased array or horn antenna to concentrate the signal in one direction. We show that mmWave signals reflected off a human body can accurately represent minute chest motion necessary to estimate human's breathing and heart rate. Due to the directional nature, the signal is not affected by any other motion outside the transmitter (Tx) and receiver (Rx) beams. Even more importantly, the directional beams reduce the signal footprint of monitor-

Permission to make digital or hard copies of all or part of this work for personal or classroom use is granted without fee provided that copies are not made or distributed for profit or commercial advantage and that copies bear this notice and the full citation on the first page. Copyrights for components of this work owned by others than ACM must be honored. Abstracting with credit is permitted. To copy otherwise, or republish, to post on servers or to redistribute to lists, requires prior specific permission and/or a fee. Request permissions from permissions@acm.org.

MobiHoc'16, July 04-08, 2016, Paderborn, Germany

© 2016 ACM. ISBN 978-1-4503-4184-4/16/07...\$15.00

DOI: <http://dx.doi.org/10.1145/2942358.2942381>

ing each human, which allows higher spatial reuse where multiple human subjects can be monitored in parallel within a room.

In this paper, we present mmVital, a comprehensive vital sign monitoring system using mmWave. mmVital can measure human's breathing rate and heart rate in different positions (standing, sitting, sleeping etc.) without requiring any proactive actions from the human. It is robust to different distances and incident angles of the impinging signal as humans can change their locations anywhere in the room. mmVital solves multiple challenges towards building a practical monitoring system. With mmWave, it is necessary to perform Tx and Rx beamforming towards the human in order to reflect the signal off her body. To address this challenge, mmVital utilizes a *human finding* process where the indoor surrounding is profiled and monitored in terms of mmWave reflections. The human finding procedure results in accurate beamforming angles to point and reflect the signal from human. We identify the separation conditions that dictate how multiple humans can be monitored using mmWave and how mmVital can provide very high concurrency of monitoring compared to the omni-directional WiFi-based solutions. This feature can facilitate parallel monitoring of multiple patients on nearby beds in a hospital room or different family members in a home. Our contributions can be summarized as follows:

(1) We empirically demonstrate the feasibility of monitoring of breathing and heart rates using 60 GHz mmWave signals. We develop a state-of-the-art testbed and design mmVital, a vital sign monitoring system that utilizes RSS of the mmWave signal reflected from the human to provide accurate vital sign monitoring while being robust to different incident angles and distances.

(2) A novel *human finding* technique is developed that can be used by mmVital to locate a user based on the reflection loss of human body. We develop a reflection loss based classification that can accurately and efficiently distinguish reflection from a human body or other objects (e.g. walls, chairs etc.).

(3) We systematically study and empirically derive (angular and distance) separation necessary between humans for concurrently monitoring their vital signs. Additionally, we establish relationships between the necessary separation and the antenna beamwidth, and outline possible cases like blockage, multiple reflections etc.

(4) We do an extensive evaluation of mmVital using our 60 GHz testbed with 7 participants in office and home environment. The mean estimation error across all participant is observed to be 0.43 breaths per minute (Bpm) and 2.15 beats per minute (bpm). The human finding procedure achieves object-human classification accuracy of 98.4% with 100 ms of dwell time on reflection changes. mmVital is also accurate in behind-the-wall breathing rate estimation with mean estimation error of 0.58 Bpm.

The rest of the paper is organized as follows. Section 2 discusses the related work. Section 3 provides the overview of mmVital and Section 4 discusses the breathing rate and heart rate estimation modules. Section 5 details the human finding procedure and Section 6 discusses the monitoring of multiple people. Section 7 provides the numerical results and we conclude in Section 8.

2. RELATED WORK

RF signal based contact-free solutions to vital sign monitoring have received increasing attention in recent years. The solutions use either 2.4/5 GHz band or 60 GHz band for sensing.

2.4/5 GHz based vital sign monitoring: The authors in [5] proposed to use WiFi RSS for respiratory monitoring. However, it requires the person to hold a device or stand in the line-of-sight path between TX and RX nodes for accurate monitoring. Liu et. al. [18] leveraged fine-grained Channel State Information (CSI) of WiFi to track vital signs. The primary focus of the work to measure the vi-

tal signs when a person is sleeping and the approach is applicable to monitoring single person in a controlled environment. Also, the proposed solution can only monitor multiple humans when their vital signs are sufficiently distinct. However, in practical scenarios, individual's vital signs can vary substantially in a short time period. A similar work [24] studied a natural setting in the home with both LOS and NLOS cases to estimate a single person's respiration rate using customized WiFi hardware. The work is limited to measuring breathing rate (not heart rate) and can only monitor multiple humans breathing rate when they are sufficiently different. A wireless sensor system using 802.15.4 devices was proposed to monitor vital signs in [22] which requires deployment of many sensor nodes/links for accurate monitoring of a single human. Adib et. al. [6] proposed to use Frequency Modulated Continuous Radio (FMCR) radar for breathing and heart rates estimation. The proposed work can monitor multiple human subjects in parallel. However, it utilizes a customized dedicated hardware with a large bandwidth of 1.8 GHz (between 5-7 GHz). In contrast, mmVital can reuse the IEEE 802.11ad commercial networking hardware for the purpose of vital sign monitoring. Although we use customized mmWave platform (due to the unavailability of off-the-shelf hardware), our techniques simply rely on RSS and can be easily implemented on low-cost future commercial 60 GHz WLAN devices.

mmWave sensing and networking: Previous works have also studied vital signs detection using mmWave signal in different frequencies, such as 228 GHz [23], 94 GHz [8, 19] and 60 GHz [9, 16]. The primary focus of these papers have been to demonstrate the feasibility of vital sign monitoring with mmWave. They assume simple controlled settings with one human subject at a close distance from the transmitter and receiver. In addition, [8] and [9] focused on the mmWave sensor and hardware/chip design for vital signs detection. In our work, we focus on solving practical challenges such as finding the human's location in a room and realizing the true to potential of directional beams by sensing multiple humans concurrently. mmVital is designed to be operational in realistic indoor environments like offices, homes etc. as shown in our evaluation. 60GHz millimeter wave sensing has been studied in literature for other applications like target tracking and activity monitoring [29]. In a recent work, [27] proposed high-precision tracking of objects (writing with pen) using mmWave beam scanning. The reflection characteristics of different objects for mmWave signals have been studied in [17]. Authors in [25] provides a link level measurement of blockage and reflection in an indoor environment, and our reflection measurements closely match their results due to similarity of 60 GHz transmitter and receiver system. 60 GHz communication has been studied for outdoor picocells [32] with its reflection and absorption characteristics, for wireless links in data center networks [31] and for WLANs with beamforming assisted via out-of-band 2.4/5 GHz WiFi [20] or via client sensors [28]. The reflection, blockage and beam-steering characteristics studied in these works are in agreement with our work.

3. SYSTEM DESIGN

We now describe our 60 GHz communication platform, design goals, challenges and provide an overview of mmVital.

3.1 mmWave Communication Platform

mmVital is implemented using 60 GHz transmitter and receiver which use a mmWave development platform provided by Vubiq [21]. The mmWave platform provides a 60 GHz RF front-end and a waveguide module as shown in Fig. 1. On the transmitter side, we use a signal generator (Keysight EXG N5172B) that produces a 10 MHz baseband signal that is input to the Vubiq transmitter mod-

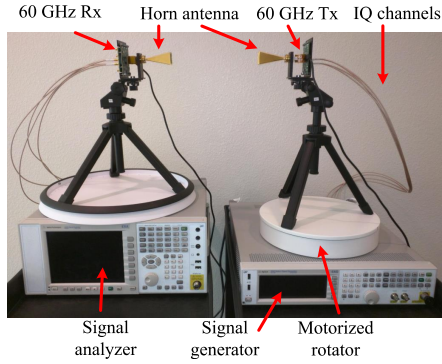


Figure 1: mmVital 60 GHz transmitter and receiver system

ule. On the receiver side, the 60 GHz receiver module is connected to a spectrum analyzer (Keysight EXA N9010A) that allows us to analyze the received baseband signal. We calculate the Received Signal Strength (RSS) using the power spectral density distribution provided by the spectrum analyzer. The RSS values are available at an average of 62 samples per second in experiment setup, which is sufficient for monitoring breathing and heart rates. Due to the unavailability of any reconfigurable phased array, we use a horn antenna with 3-dB beamwidth of 12° (estimated first null beamwidth (FNBW) of 24°) and 24 dBi gain on the transmitter and receiver. A mechanical rotator is used to form the beams in different directions and scan the surroundings for reflections.

3.2 Design Goals and Challenges

To compensate for high attenuation loss, 60 GHz radios use directional antenna (e.g. horn antenna or phased array). The central objective of mmVital is to exploit the directional nature of mmWave communication to accurately measure human's breathing and heart rates. The mmWave Tx directs its signal to the human body and the reflected signal is received by the Rx. In terms of design, mmVital should be able to exploit the directional nature of mmWave and measure the vital signs of *multiple humans* concurrently. mmVital should be *non-invasive*, which means that it should not require the human to perform any specific actions to monitor the vital signs. mmVital should also be *ubiquitous* where the monitoring can be performed anywhere within the reach of Tx and Rx. Additionally, the monitoring should be accurate even when human is sleeping, standing or sitting, and should be robust to different postures (front, back, right and left). Although the directional nature of 60 GHz communication reduces the inaccuracies introduced by other motions and indoor multi-paths, it also raises multiple challenges -

(1) Because a human can be at different places compared to the Tx and Rx, it is necessary that the reflection-based monitoring is robust to different incident angles of signal onto the human body and different postures (front, back, left, right) of the body. We study the impact of incident angle and body postures on vital sign monitoring.

(2) Before starting the vital signs monitoring, it is first required to *find* the human in the vicinity of Tx and Rx. Since various indoor objects (e.g. wall, metal cabinet etc.) reflect the mmWave signal, mmVital needs to distinguish the reflections from objects and humans. Although this can be accomplished by inspecting each reflection for heartbeats, the time overhead of such inspection with many possible reflections indoors can be very high. We develop an algorithm for *human finding*, where the Tx and Rx engage in an iterative scanning to profile indoor environment in terms of its current reflections, and inspect them to identify the reflection from human body.

(3) With narrow beamwidths, it is possible to use multiple non-

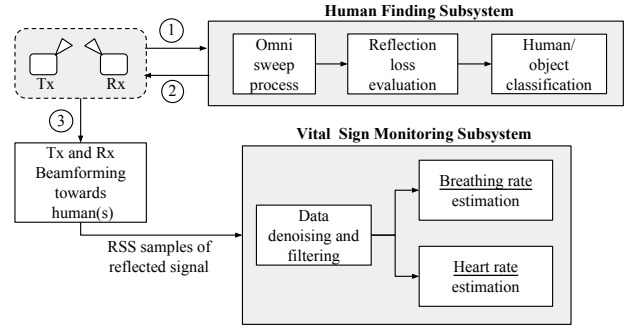


Figure 2: Overview of mmVital

overlapping beams to monitor the vital signs of multiple humans in parallel. Relative position of multiple humans result in many complex reflection scenarios such as blockage of one human by the other or multiple reflections. We systematically classify various scenarios and study the angular and distance separation necessary for concurrent sensing.

3.3 System Overview

Various components of mmVital are shown in a block diagram in Fig. 2. At a high level, mmVital contains two subsystems - (i) Human finding subsystem and (ii) Vital sign monitoring subsystem. The goal of the former subsystem is to find the human in a room (or an indoor space) so that Tx can direct its signal towards the human and Rx can receive the reflection. For accomplishing this efficiently, mmVital utilizes an omni-sweep procedure that profiles the indoor environment in terms of its reflections and tracks any changes to it. When new reflections are detected, the reflection loss is evaluated to classify if they are from movable objects (e.g. chairs, laptops etc.) or a human. mmVital leverages the diversity in material permittivity to accurately identify human reflections. Once the Tx and Rx beamforming angles towards the human are determined, the second subsystem performs the vital sign monitoring. Here, the signal reflected by the human body are analyzed through RSS samples to estimate the vital signs. The RSS samples first undergo data denoising procedure where a sliding window-based moving average filter is applied to remove the high-frequency noise. Apart from that, we also apply a bandpass frequency filter with cutoff of 0.1-20 Hz in order to remove the impact of slow moving DC component as well as moderate to high frequency human movements [26] (e.g. shaking of body parts). The breathing rate and heart rate modules further apply their custom filters and peak detection algorithms (discussed in the next section) for estimation. We first provide the details of vital signs subsystem in the next section and defer to the discussion on human finding subsystem to Section 5.

4. MEASURING VITAL SIGNS

4.1 Breathing and Heart Rates

In order to estimate the breathing rate, we transform the filtered RSS data to frequency domain. We observe that the RSS signal is very sensitive to periodic movement of human breathing, which results in a peak (dominant frequency) in the frequency domain. The frequency of the peak represents the breathing rate at a coarse-grain. However, simply selecting the highest peak is not always accurate due to variations introduced by noise and motion. To achieve a better accuracy, we select the highest magnitude peak as well as the frequency of the two adjacent bins, and create a custom narrow band-pass filter. We apply the filter on the RSS data and perform an Inverse FFT (IFFT) to yield the filtered time-series data. We then use a simple peak detection algorithm for precisely counting

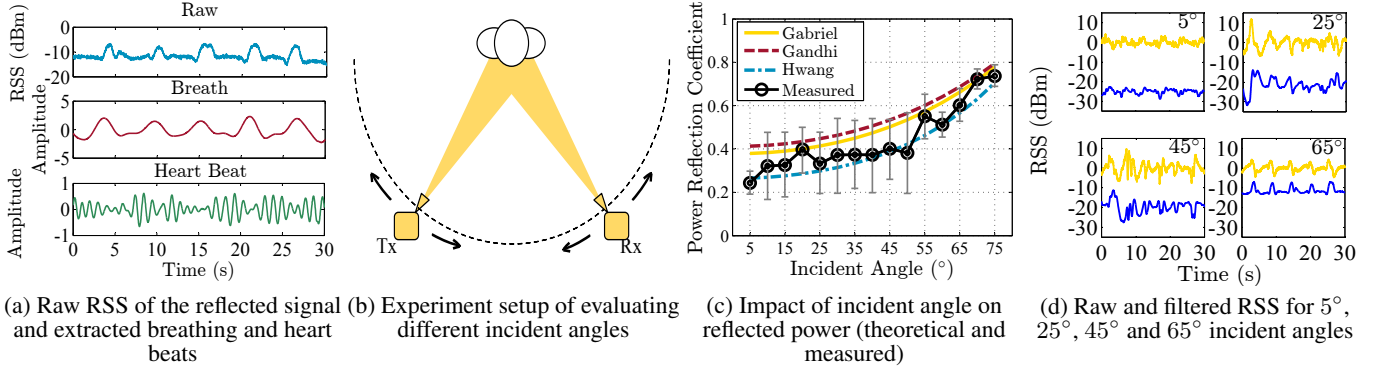


Figure 3: RSS of reflected signal, extracted breaths and heart beats, and impact of incident angle

the breathing rate in Bpm.

The normal heart rate of an adult is known to be in the range of 60-100 [12] bpm. However, during high-intensity activities like exercising, the heart rate can exceed 170 bpm [12]. For such activities and to detect any other abnormal conditions, we select the heart rate range to be 50-220 bpm. Similar to the breathing rate estimation, we apply an FFT on the RSS time-series data and determine the dominant frequency. In this case, we select the highest magnitude peak along with four adjacent bins of frequency to create the custom band-pass filter because the heart beat motion is smaller compared to the breathing motion and can exhibit larger variations. We apply the filter, perform IFFT and use the peak detection for estimating heart rate.

Fig. 3a shows an example of raw RSS samples along with filtered breathing and heart beat samples. We offset the RSS values by the transmission power to present the RSS and RSS loss on the same scale. After applying the customized filters, we apply peak detection algorithm for accurate counting. We note the mmVital estimates the vital signs in real-time using a sliding window of 30 seconds offset by approximately 100ms (every 6 RSS samples in our testbed).

4.2 Impact of Incident Angle

Because a human can be anywhere within the Tx and Rx vicinity while being monitored for her vital signs, the transmitted signal can impinge on the human body at any angle (referred as incident angle). We now investigate the impact of incident angle on the reflected signal, and the robustness of breathing rate and heart rate estimation. The amount of energy reflected from an object can be quantified using *power reflection coefficient* which can be derived from reflection coefficient. The reflection coefficient is the ratio of the complex amplitude of the reflected electromagnetic wave to that of the incident wave. The coefficient depends on factors such as the permittivity (a complex value) of the object material and the signal incident angle. The reflection coefficient (r) can be calculated [7] as

$$r = \frac{1 - e^{-j2\omega}}{1 - r_i e^{-j2\omega}} r_i, \quad \text{for } i \in \{\perp, \parallel\} \quad (1)$$

where $\omega = \frac{2\pi l}{\lambda} \sqrt{\epsilon_2/\epsilon_1 - \sin^2 \gamma}$, l denotes the thickness of the reflecting source; λ denotes the signal wavelength; γ is the incident angle; ϵ_1 and ϵ_2 are the permittivities of the first medium and the second medium, respectively. In a simplified single layer model, the first medium can be assumed as air which has the permittivity of 1. r_{\perp} and r_{\parallel} are the Fresnel's reflection coefficients when the electric field is perpendicular and parallel to the incidence plane, respectively. The coefficients can be calculated as

$$r_{\perp} = \frac{\cos \gamma - \sqrt{\epsilon_2/\epsilon_1 - \sin^2 \gamma}}{\cos \gamma + \sqrt{\epsilon_2/\epsilon_1 - \sin^2 \gamma}}. \quad (2)$$

$$r_{\parallel} = \frac{\epsilon_2 \cos \gamma - \sqrt{\epsilon_2 \epsilon_1 - \epsilon_1^2 \sin^2 \gamma}}{\epsilon_2 \cos \gamma + \sqrt{\epsilon_2 \epsilon_1 - \epsilon_1^2 \sin^2 \gamma}}. \quad (3)$$

The reflection coefficient (r) can be used to estimate the power loss due to reflection (or power reflection coefficient) as $L_R = \frac{P_O}{P_I} = |r|^2$ where P_O and P_I are the values of reflected (after reflection) and incident (before reflection) power respectively.

We empirically evaluate the impact of incident angle on the reflection power loss as shown in Fig. 3b. In the experiments, the Tx and Rx move symmetrically on a circle of 3 meter radius. The human sits at the center of the circle, and both Tx and Rx point their horn antennas to the human. Since the P_I is unknown, we first use an aluminum plate at each incident angle in the place of the human and measure the received power. As an aluminum plate is regarded as a perfect reflector (reflection loss nearly 0 dB), and we use its received power as a reference for human measurements. Fig. 3c shows the reflection loss (L_R) for incident angles from 5° to 75°. It also compares the theoretical value of reflection loss calculated using Eq.1 and 2 (perpendicular). For the calculations, three different values of human body/skin permittivity are considered based on previous work from Gabriel et al. [10], Gandhi et al. [11] and Hwang et al. [14]. These values are $7.89 - j10.90$, $8.89 - j13.15$ and $8.05 - j4.13$ at 60 GHz, respectively [30]. We observe that our measurements are in agreement with permittivity models of [10] and [14]. Higher variations observed in the measurements are due to human's breathing motion. Examples of the reflected RSS (raw and filtered) at different incident angles are shown in Fig. 3d. It can be seen that as the incident angle increases, the RSS samples becomes less and less noisy mostly due to decrease in the reflection loss. The main observation in Fig. 3d is that the reflected RSS is representative of the breathing motion at all incident angles. Hence, mmVital is robust to human changing location relative to Tx and Rx. Also, if mmVital is used to monitor humans when they do not change location (e.g. sleeping in bedroom or hospital bed), it is advisable to deploy the Tx and the Rx at larger incident angles to increase the estimation accuracy. We will evaluate the vital sign estimation accuracy for multiple human subjects with different incident angles in Section 7.

5. HUMAN FINDING

A major challenge in the design of mmVital is that it is required to determine where the human is before it can start monitoring her vital signs. In home, office or a similar indoor place where human can freely move from one place to another, mmVital should be able to *find* the human and point the transmitted signal towards her body. In this section, we introduce a *human finding* procedure that can be used to determine precise Tx and Rx angle to transmit the signal to human body and receive the reflection respectively. The challenge of human finding is further complicated by the fact that

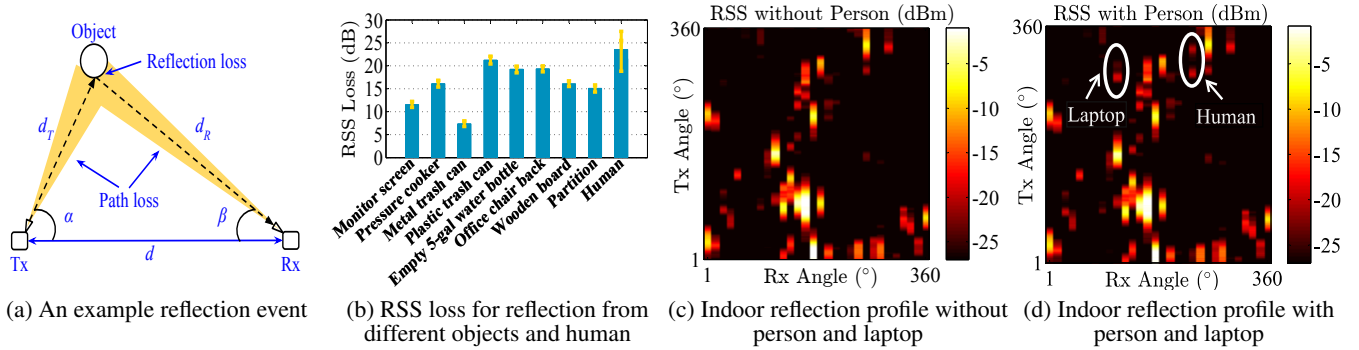


Figure 4: Reflection loss for different types of objects and reflection profile of a room

60 GHz signal is reflected by many different objects in an indoor environment. Such objects include walls, metal objects such as cupboards, monitors, microwave, trash-cans etc. In the presence of many possible reflections, it is difficult for the Tx and Rx to know which reflection is indeed coming from a human.

mmVital utilizes a novel approach to distinguish human from objects based on reflective loss as it is known to be different for different objects [17]. The permittivity dictates the amount of signal that penetrates the object and reflects from it. Apart from penetration and reflection, the signal is also absorbed by the objects and scattered from its surface. However, absorption and scattering effect are difficult to measure in our system. Instead, mmVital leverages the difference in reflection loss due to different permittivity to distinguish the objects from human.

In order to measure the reflection loss, it is first necessary to remove the effect of distance dependent path loss. Fig. 4a shows an example reflection event from an object. If the transmission power is P_T , transmit antenna gain is G_T , received power is P_R , and receiver antenna gain is G_R , the total loss $L = (P_T + G_T + G_R) - P_R$ is as follows

$$L = L_P(d_T) + L_P(d_R) + L_R(\epsilon_o) \quad (4)$$

where $L_R(\epsilon_o)$ is reflection loss from object with permittivity of ϵ_o , d_T and d_R are the distances of the object from the Tx and Rx respectively. The reflection loss can be calculated as shown in Section 4.2. The path loss $L_P(D)$ at distance d can be calculated using Friis model of free-space attenuation as

$$L_P(D) = 20 \log_{10} \left(\frac{4\pi D}{\lambda} \right) \quad (5)$$

where λ is the signal wavelength. The Tx and Rx have the knowledge of P_T and P_R , and the distance between them (d). As shown in Fig. 4a, d_T and d_R can be calculated using the angle of transmission (α) and reception (β) to derive $L_P(d_T)$ and $L_P(d_R)$. Using Eq. 4 and 5, they can calculate the reflection loss $L_R(\epsilon_o)$. The reflection loss can then be used to distinguish if the reflection is coming from a human or an object.

To evaluate the feasibility of object/human classification based on reflection loss, we test a variety of reflective objects and place them at one fixed location (fixed path loss) one by one. The observed RSS values for the objects and human are shown in Fig. 4b. We can observe that different objects and human, depending on their material permittivity, reflects different amount of signal. Hence, we use regression on the reflection loss to identify if it is from an object or a human. In our experiments, we observe that the human/object classification can be done using even a single RSS sample based on the reflection loss, making the human finding procedure very efficient. With the use of more RSS samples, the confidence of classification can be further improved since the RSS for human reflected signal varies more due to heartbeat and breathing

Algorithm 1 Human Finding Procedure

Input: Tx power (P_T), RSS variation tolerance threshold (κ), Beam sweep step size (s°), number of previous RSS samples (k), Human/object classifier ($\Psi(\cdot)$), distance between Tx and Rx (d)

Output: Tx and Rx angles towards human

Procedure:

```

1: for  $\alpha : 0^\circ \rightarrow 360^\circ$  do #Omni-sweep procedure
2:   for  $\beta : 0^\circ \rightarrow 360^\circ$  do
3:      $R_{(\alpha,\beta)}^t = RSS(\alpha, \beta)$ 
4:      $\Delta_{(\alpha,\beta)}^t = |R_{(\alpha,\beta)}^{t-1} - R_{(\alpha,\beta)}^t|$ 
5:     if  $\Delta_{(\alpha,\beta)}^t > \kappa$  then #Change in reflection
6:       Calculate  $d_T$  and  $d_R$  using  $\alpha, \beta$  and  $d$ 
7:       for  $i : t - k \rightarrow t$  do #Analyze last k samples
8:          $L_{(\alpha,\beta)}^i = P_T - R_{(\alpha,\beta)}^i - L_P(d_T) - L_P(d_R)$ 
9:          $\Gamma_{(\alpha,\beta)} = \Gamma_{(\alpha,\beta)} \cup L_{(\alpha,\beta)}^i$ 
10:      end for
11:      if  $\Psi(\Gamma_{(\alpha,\beta)}) = \text{"Human"}$  then #Human-object
12:        return  $\alpha, \beta$  #classification
13:      end if
14:    end if
15:     $\beta = \beta + s^\circ$ 
16:  end for
17:   $\alpha = \alpha + s^\circ$ 
18: end for

```

motion compared to the objects.

Before the classification can be applied, mmVital is required to find the reflection profile of the indoor environment. The reflection profile can be found by a brute-force omni-directional sweeping of Tx and Rx beams. The procedure is formally described in Algorithm 1. For each Rx angle (in steps from 0° to 360°), the Tx scans the entire 360° to determine all reflections. Note that although the omni-sweep procedure is brute-force, it can be completed in a short time with digital beamforming where beam switching can be performed at much smaller time scales. Also, the procedure is only required to be performed when human's vital signs can no longer be monitored and human finding procedure has to be initiated. Also, both Tx and Rx can use discrete steps for angle increment for generating non-overlapped beams (similar to sectors in 802.11ad) to reduce the time complexity.

To demonstrate the omni-sweep procedure, we use our testbed to build the reflection profile of a room. Due to our horn antenna 3-dB beamwidth of 12° , the Rx scans all directions in increments of 12° . For each Rx angle, Tx scans the entire 360° with continuous rotation. The reflection profile in the absence of any human is shown in Fig. 4c. As we can see, a typical room has many different reflections from wall and other objects. In mmVital, the profile

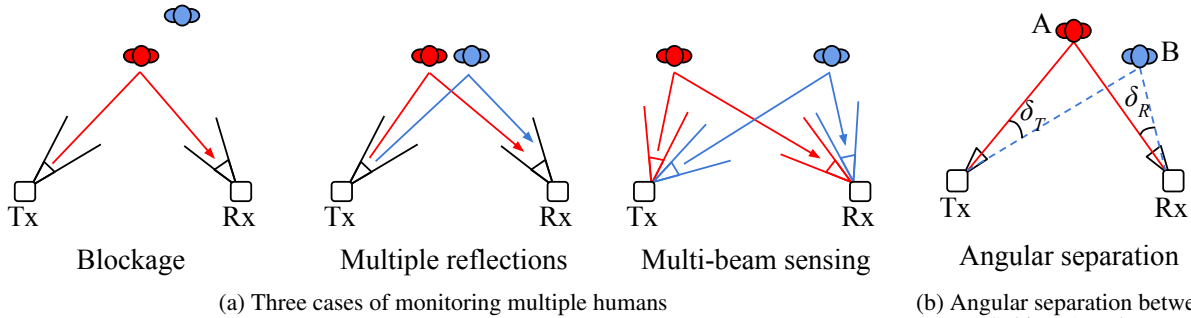


Figure 5: (a) Relative position of humans compared to Tx and Rx gives rise to three cases - blockage, multiple reflections and multi-beam sensing (b) Angular separation between two humans can be calculated as $\min(\delta_T, \delta_R)$

can be built in the absence of a human and then only the changes in reflections need to be monitored to find human. Note that a change in reflection can occur due to the presence of a human (increase if new reflection and possible decrease if existing reflection blocked) as well as movement of any existing object (e.g. moving a chair or laptop). Fig. 4d shows the reflection profile with a human and a laptop (with metal enclosure) in the room. Both laptop and human reflect the signal, which can be tagged as the change in the reflections. As in Algorithm 1, each change in reflection is inspected using the reflection-loss based classifier to identify if the change is due to a human or an object. As we observe from Fig. 4d, in some cases, the existing reflections exhibit minor difference in RSS at different times. This can be due to the changes in object temperature. In order to ignore such minor variations, we utilize a RSS variation tolerance threshold (κ). Whenever a change in RSS is within the threshold, mmVital does not consider the reflection for object-human classification. Lastly, for the changed reflections, the Tx and Rx angles are used to determine the path loss, and calculate the reflection loss as Eq. 4. This reflection loss is input to the object-human classifier, and if the reflection loss is classified as “human”, the Tx and Rx angles of the reflections are used to start monitoring the human for her vital signs.

6. MONITORING MULTIPLE HUMANS

Due to the directional nature of 60 GHz communication, it can monitor multiple humans in a room concurrently. Monitoring multiple humans is useful in many practical scenarios. For example, more than one family members in a house or multiple patients in hospital room can be monitored in parallel using the same mmWave Tx-Rx pair. In this section, we first systematically categorize various scenarios of monitoring multiple people with mmWave and then study how much separation between humans is necessary to sense their vital signs in parallel.

6.1 Single and Multi-Beam Sensing

The cases of monitoring multiple humans can be classified as follows (refer to Fig. 5a) -

(1) **Single-Beam Sensing:** In single-beam sensing, two (or more) humans are monitored with the use of only one pair of fixed Tx and Rx beams without any switching of beam direction. These cases can be further classified in two classes -

a) *Blockage* where one human blocks the other human completely, allowing only one human to be monitored at a time.

b) *Multiple reflections* where mmWave signal is reflected partially from both the humans. With multiple reflections, it is possible to sense the vital signs both the humans if they have distinct heart and breathing rates. Most of the current 2.4/5 GHz RF-based vital sign monitoring research [5, 18, 24] assume such distinct vital sign monitoring for all users within the omni-directional range of the

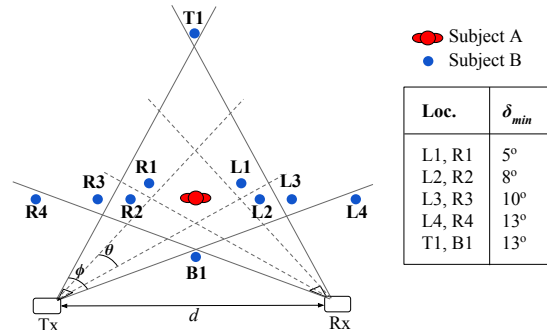


Figure 6: Experiment setup used for evaluating the impact of angular separation

Tx and Rx. However, in reality, multiple users can have similar vital signs and even the vital signs vary substantially over time. With mmVital, such restrictions of distinct vital signs are limited only to a small region within the beams.

(2) **Multi-Beam Sensing:** When there is a second human outside the Tx and Rx beams of the first human being monitored, both of them can be monitored by switching the beams between the two at a fast rate (using digital beamforming in nanoseconds). We refer to such cases as *multibeam monitoring* (Fig. 5a), where multiple non-interfering beams are used by the Tx and Rx to monitor people outside the beams of each other.

6.2 Human Separation

We now study the separation necessary between two humans for all cases of single and multi-beam sensing. In order to characterize the spatial reuse (from sensing perspective) in the area of interest, we identify two types of separation - angular and distance. As shown in Fig. 5b, let δ_T denote the angle between the straight lines connecting Tx to human A and human B. Similarly, let δ_R denote the angle between the straight lines connecting Rx to human A and human B. The *angular separation* (δ_{min}) is defined as $\min(\delta_T, \delta_R)$. The *distance separation* (s) is simply calculated as the Euclidean distance between human A and human B.

6.2.1 Angular Separation

We now empirically derive a relationship between the minimum required angular separation and the antenna beamwidth. In our experiment setup (Fig. 6), one human (A) stands in the center with Tx and Rx pointing their beam to her. Another human (B) changes her position from L_1 to L_4 and R_1 to R_4 to vary the angular separation from 5° to 13°. Recall that in our testbed, the FNBW $\phi \approx 24^\circ$ and 3-dB beamwidth $\theta = 12^\circ$. We intentionally ask Humans A and B to breathe at different rates (Human A at 8-11 Bpm and Human B at 21-27 Bpm) in order to make their breathing rates distinguishable in the frequency domain. We repeat the setup and experiments

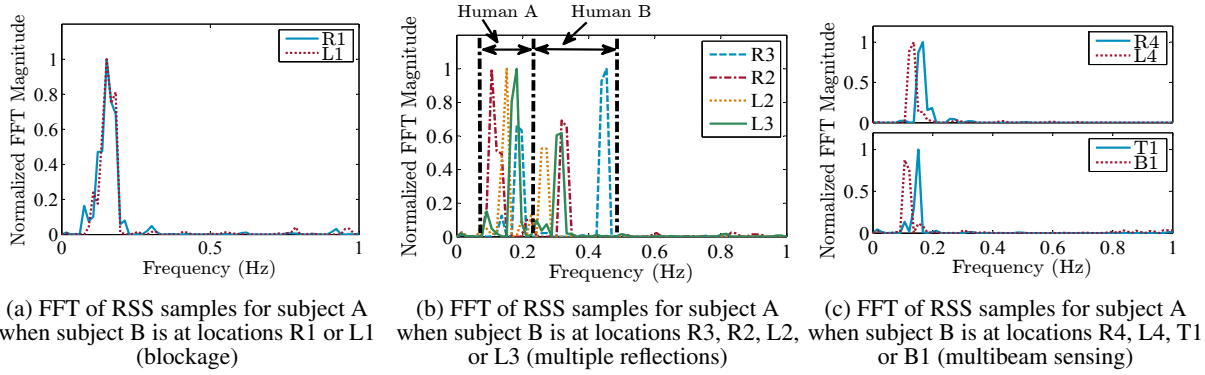


Figure 7: FFT of RSS samples for subject A when subject B stands at different locations (Fig. 6) to create blockage, multiple reflections and multi-beam sensing scenarios



Figure 8: Schematic showing physical regions of blockage, multiple reflections and multi-beam sensing

in three different rooms for verification.

Figs. 7 show normalized FFT of the received RSS for the 10 cases. We choose locations L_1 and R_1 to emulate blockage scenarios where either signal is blocked by Human A before it reaches Human B (L_1) or signal reflection from Human B (R_1) is blocked by Human A before it reaches the receiver. We observe from Fig. 7a that for Locations L_1 and R_1 of Human B, only Human A's breathing can be detected from the reflected RSS.

For locations L_2, L_3, R_2 and R_3 , the transmitted signal is reflected from both Humans A and B (multiple reflections). This can be seen as FFT peaks around 0.23-0.45 Hz (Human B) and 0.13-0.18 Hz (Human A) in Fig. 7b. It shows that vital signs of both humans can be calculated by applying appropriate frequency band-pass filters.

At locations L_4, R_4, T_1 , and B_1 , no breathing of Human B is detected in Fig. 7c, indicating that Human B is outside the Tx and Rx beams being used for human A. For these cases, both A and B can be monitored by switching the beams between them in time.

The following relationship between the angular separation and the beamwidth is observed from the above experiments. It is also schematically shown in Fig. 8.

(1) Blockage: when the angular separation between two humans is less than half the 3dB beamwidth of antenna $0 \leq \delta_{min} \leq \frac{\theta}{2}$, one human is likely to block the signal from impinging the other human.

(2) Multiple reflections: when the angular separation between two humans is $\frac{\theta}{2} \leq \delta_{min} \leq \frac{\phi}{2}$, both humans can be monitored in parallel as long as their breathing/heart rates are different.

(3) Multi-beam sensing: when $\delta_{min} > \frac{\phi}{2}$, both humans can be monitored by switching the beams between the two at a fast rate.

6.2.2 Distance Separation

The angular separation is essential to understand the conditions that dictate single and multi-beam sensing cases. However, it does not provide sufficient insight in how much physical distance is re-

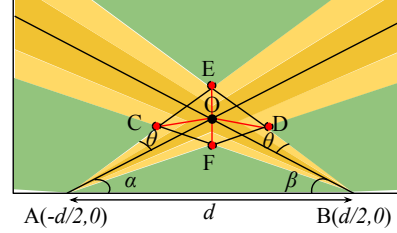


Figure 9: Four nearest locations where another human can be present without interfering with the target human at Point O

quired between two humans for parallel sensing. In this section, we study distance separation and derive its relationship with beamwidth and relative positioning of Tx, Rx and human subjects.

Fig. 9 shows an example setup where the Tx and Rx pair is monitoring a human at location O. Let $\alpha = \angle OAB$ and $\beta = \angle OBA$ indicate the Tx and Rx beam directions respectively. We assume that Tx is located at Point $A(-d/2, 0)$ and Rx is located at Point $B(d/2, 0)$ where d is the distance between Tx and Rx. We can observe from Fig. 6 that another human can be at four nearest locations (points $C(x_C, y_C)$, $D(x_D, y_D)$, $E(x_E, y_E)$ and $F(x_F, y_F)$ in Fig. 9) for multi-beam sensing. Here, we primarily focus on multi-beam sensing cases as it is more practical compared to multiple reflection cases which occur in relatively smaller area and also require the users' vital signs to be different. We define the distance separation (s) to be the minimum of the four distances OC , OD , OE and OF . The distance s indicates the best-case of minimum separation necessary between the two humans. It is dependent on α , β and ϕ (FNBW), and can occur in any direction from the human at location O.

The four distances OC , OD , OE and OF can be calculated by deriving the coordinates of the points in the 2-D Euclidean space. Note that we assume $\theta = \frac{\phi}{2}$ because the 3 dB beamwidth can be approximated as half of FNBW in most mmWave horn antennas. Using these, X and Y coordinates of point O (when $\theta < \alpha$, $\theta < \beta$) can be calculated as

$$x_O = \frac{-d}{2} + \frac{d \cos \alpha \sin \beta}{\sin(\alpha + \beta)}; \quad y_O = \frac{d \sin \alpha \sin \beta}{\sin(\alpha + \beta)}. \quad (6)$$

The complete derivation of the coordinates of points and four distances can be found in [4]. We use them to calculate the best-case distance separation (s^*).

In the experiment setup of Fig. 6, we also evaluate two additional locations (T_1 and B_1) for human B. As we observe from Fig. 7c, we observe that presence of human B is not detected in the FFT which means that it has a sufficient distance separation from human A to allow multi-beam sensing. We also evaluate the best-case distance separation for all points in a room of $10m \times 10m$ and

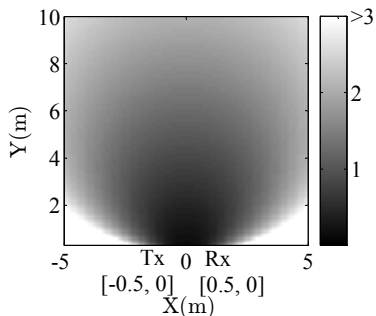


Figure 10: Best case distance separation in a $10m \times 10m$ room

the results are shown in Fig. 10. We find that for majority of locations within the room, the value of s^* is relatively small (median = 1.67 meters) which indicates that mmVital in our testbed setup can monitor multiple humans even when they are relatively close to each other.

7. EVALUATION

We perform an extensive evaluation of mmVital in two different indoor scenarios as shown in Fig. 11. First room is a laboratory room (size: $6m \times 9m$) in a university building with objects such as cubicle partitions, white boards, metal cupboard, computers etc. The second room is an apartment bedroom of size $4.5m \times 6m$ with a bed in the center and other furniture on the sides. Fig. 11 shows the positions of Tx and Rx. We enroll 7 participants over a period of two weeks to monitor their vital signs. Out of the 7 subjects, 6 subjects had a Body Mass Index (BMI) of $19-25 \text{ kg/m}^2$ and one subject (Subject #6) had the BMI of 29 kg/m^2 . The BMI is correlated with breathing rate and other cardiovascular parameters [1]. The ground truth is established using a finger pulse oximeter [3] (for heart rate) and Neulog chest-strap respiration monitor [13].

7.1 Accuracy of Vital Sign Monitoring

7.1.1 Breathing and Heart Rate Estimation Accuracy

For evaluating the breathing and heart rates of participants, we use three different incident angles in the university room. Figs. 12a and 12b show the mean estimation error with (95% confidence intervals) for breathing rate (Bpm) and heart rate (bpm) for the 7 participants at 3 different incident angles (70° , 50° , 30°). The accuracy is calculated for 3 experiment runs of 10 minutes for each of the participants. For the incident angle of 70° , the mean estimation error in breathing rate and heart rate estimation is less than 0.5 Bpm and 2.5 bpm respectively for all 7 participants. This shows that 60 GHz vital sign monitoring can provide highly reliable estimate of breathing and heart rates. The estimation error increases with the decrease in the incident angles, which proves the relationship between the reflection loss and incident angle discussed in Section 4.2. At higher incident angles, the reflection loss decreases as well as the reflected RSS is observed to be less noisy. Both these factors increase the vital sign estimation accuracy. We observe that the breathing and heart rate estimation errors are slightly higher for Subject #6 which is likely due to higher BMI. Since these experiments were performed with the participants either standing or sitting, the estimation error is likely to be even lower when they are sleeping on bed as breathing rate is substantially more stable when human is sleeping.

7.1.2 Robustness to Distance and Posture

We also evaluate the impact of human's distance from Tx and Rx on the observed RSS and the accuracy of vital sign monitoring. The estimation accuracy is defined as the difference between the ground

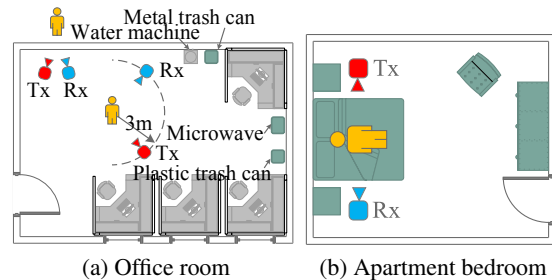


Figure 11: Experiment setup in office and home

truth and the estimated vital sign divided by the ground truth. We fix the incident angle to be 45° and the location of the human subject, while moving the Tx and Rx away from the human in steps of 1 meter. We evaluate the RSS and breathing rate estimation accuracy while varying the Tx-human (and Rx-human) distance from 1 meter to 10 meters. Fig. 12c shows RSS loss and breathing rate estimation accuracy for varying distance. Note that distance in Fig. 12c indicates the Tx to human (or human to Rx) distance, so the total signal propagation distance (Tx to human and human to Rx) is actually double. As expected, the RSS loss increases and estimation accuracy decreases with increase in distance. The confidence intervals on RSS loss indicates that sufficient variations in the signal is observed even at a larger distances (upto Tx-human distance of 8 meters). Recall that this signal variation is useful in finding the human and distinguishing its reflection from other objects (Section 5). For distances lower than 8 meters, the mean breathing rate estimation error is less than 0.42 Bpm (mean accuracy is 98.8%), and beyond 8 meters the mean estimation error drops close to 1.07 Bpm, (mean accuracy is 97%). This shows vital sign estimation of mmVital is robust to distances common in rooms of typical indoor spaces like offices and homes.

Since the signal can impinge anywhere on the human body depending on the human's orientation relative to the Tx and Rx, we evaluate the impact of human's facing direction (or posture) on breathing and heart rate estimation accuracy. In this experiment, 5 participants are asked to sleep on the bed in the apartment bedroom (Fig. 11b) for 3 minutes (repeated 10 times) in four different postures - sleeping on back (Front), sleeping on stomach (Back), facing left (Left) or facing right (Right). The results of breathing rate and heart rate estimation accuracy are shown in Fig. 12d. We observe that highest breathing rate estimation accuracy is observed for the front posture in which the signal directly strikes and reflects from human's chest area which exhibits the maximum breathing motion. However, for the other three postures also breathing rate estimation accuracy remains close to 98%. In terms of heart rate estimation, front posture also provides highest accuracy, followed by the back posture. In both front and back postures, reflected signal better captures the heart beat motion compared to left and right postures. When the human is facing right, her heart is towards the incoming signal from the Tx compared to when she is facing left, resulting in a better heart rate estimation accuracy for the right posture. In all cases, we observe that mmVital achieves high vital sign monitoring accuracy even when human is in different postures.

7.1.3 Behind the Wall Estimation

The breathing rate estimation accuracy is evaluated for behind-the-wall case shown in Fig. 11a. Here, a human stands on the other side of the wall from the Tx-Rx pair. Because penetration loss and reflection loss change depending on the incident angle, two incident angles (10° , 20°) are evaluated. The mean estimation error of breathing rate is observed to be 0.58 Bpm and 0.93 Bpm for 10° and 20° , respectively. In contrast to line-of-sight cases, increase in incident angle increases the estimation error in behind-the-wall

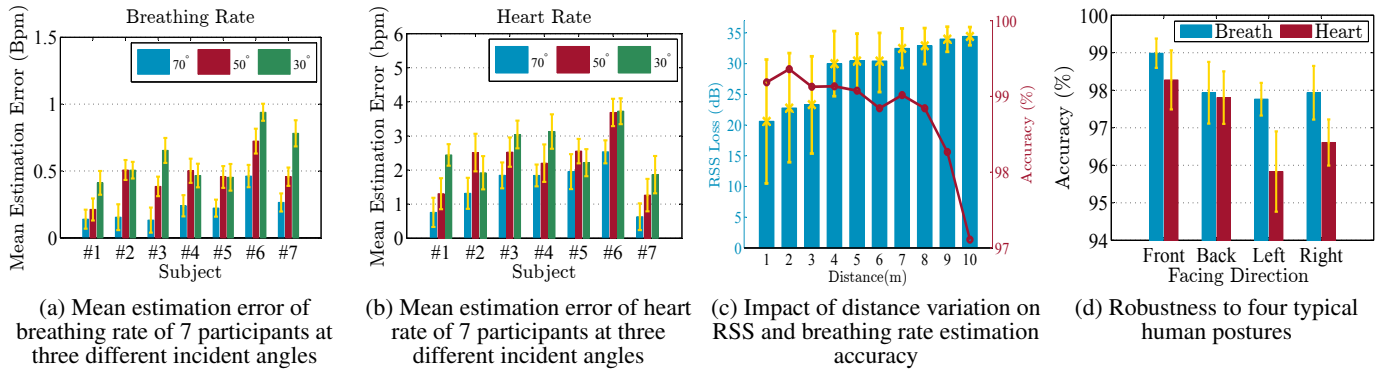


Figure 12: Accuracy of breathing rate, heart rate, impact of distance apart, and robustness to different postures

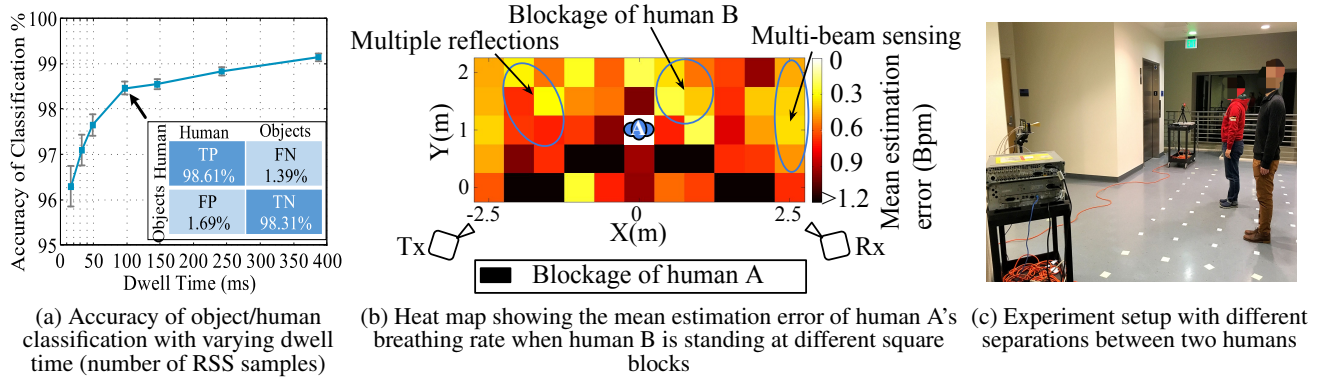


Figure 13: Accuracy of human finding and multiple people

cases. This is because at higher incident angles, more signal is reflected and lesser signal penetrates through the wall to strike human body. The RSS reflected also undergoes the same phenomenon and the received RSS carries a weaker signature of breathing motion. It is worth noting that if the application does not require behind-the-wall monitoring, the transmission power can be reduced or larger incident angles can be used (more reflection, less penetration) to contain the 60 GHz signal within the room.

7.2 Reflection Loss based Human Finding

The human finding procedure described in Algorithm 1 is evaluated in the laboratory room scenario. We create 20 different scenarios where 8 objects (laptop, metal utensil, plastic trash can, metal trash can, empty 5 gal. water bottle, chair, wooden board, partition board) and a human subject are randomly relocated inside the room. Similarly, Tx and Rx are also moved to randomly chosen points in the room. The movement of objects, human and Tx-Rx ensures that a wide variety of distances and incident angles are evaluated for moving as well as non-moving objects (walls, tables etc.). For each of 20 the scenarios, we find the reflection profile to determine the reflection from moved objects and the human. The reflection loss based classification is then applied to the RSS values of changed reflections as described in Section 5. The results of the classification are presented in Fig. 13a. We vary the time interval for which RSS samples are collected (dwell time) at each angle before performing the classification. It can be observed that as the dwell time increases, the accuracy of human-object classification increases. A reflection is from a human or an object can be determined with average accuracy of 96.2% only with one RSS sample (available after 16 ms). With 100 ms of dwell time, the accuracy increases to 98.4% with false positive rate of $< 2\%$. This means that the human finding procedure is highly robust to environment changes and can accurately determine the Tx and Rx angles for monitoring.

7.3 Monitoring Vital Signs of Multiple People

To evaluate the accuracy of vital sign estimation for multiple people using mmVital, we carefully design an experiment as shown in Figs. 13b and 13c. In this setup, we choose a rectangular area of $6m \times 2.5m$ in which human subject A stands at the center of the rectangle. The Tx and Rx point their antenna beams towards human A. We then ask human B to stand at different $0.5m \times 0.5m$ square blocks within the rectangle. In order to create and detect all of scenarios we proposed in Section 6, we ask both the subjects to intentionally breathe at different rates. For each position of human B, we estimate the breathing rate of human A. Fig. 13b shows a heat map where the color of each square block indicates human A's mean estimated breathing rate error, when human B is standing in the square. Note that human A's location remains unchanged during the experiment.

In Fig. 5a, the signal transmitted towards or reflected from human A is affected by the presence of human B at different positions, resulting in (1) blockage, (2) multiple reflections and (3) multi-beam sensing cases as discussed in Section 6. For the case that human B is between Tx and human A (the black blocks), the transmitted signal does not reach human A, resulting in blockage of human A. When human B is close to human A, transmitted signal is reflected from both the humans (multiple reflections). However, due to the presence of human B, the mean estimation error of breathing rate of human A drops close to 0.9 Bpm (four adjacent positions of human A). For many locations when human B is sufficiently far from human A, it does not interfere with the vital sign monitoring (multi-beam sensing). This means that human B is outside the current Tx and Rx beam of human A (angular separation higher than half of the FNBW), and multiple separate Tx-Rx beam pairs can be used to monitor both humans. Due to the unavailability of digital beamforming phased array antenna for 60 GHz, we leave the evaluation of multiple humans through fast switching Tx-Rx

beams to future work.

8. CONCLUSIONS

In this paper, we presented mmVital, a vital sign monitoring system utilizing mmWave signal reflected from human body. mmVital is shown to be accurate in monitoring breathing and heart rates. We also proposed a novel human finding procedure that can locate human body before vital sign monitoring using reflection loss characteristics. We evaluated mmVital using state-of-the-art 60 GHz testbed and 7 participants, and showed that it can provide accurate and robust (to incident angles and distances) vital sign monitoring. mmVital is also shown to be effective in monitoring multiple people in parallel as well as behind the wall subjects. In our ongoing research, we are exploring human movement tracking through mmWave and other smart home applications.

9. REFERENCES

- [1] BMI and Respiratory Function. <http://www.livestrong.com/article/84685-bmi-respiratory-function/>.
- [2] Intel Gigabit Wireless. <http://www.intel.com/content/dam/www/public/us/en/documents/product-briefs/tri-band-wireless-ac17265-brief.pdf>.
- [3] NeuLog Sensors. <https://neulog.com/>.
- [4] Technical Report. <http://spirit.cs.ucdavis.edu/pubs/tr/zhicheng-MobiHoc16-techReport.pdf>.
- [5] H. Abdelnasser, K. A. Harras, and M. Youssef. UbiBreathe: A Ubiquitous non-Invasive WiFi-based Breathing Estimator. In *MobiHoc '15*.
- [6] F. Adib, H. Mao, Z. Kabelac, D. Katabi, and R. C. Miller. Smart Homes that Monitor Breathing and Heart Rate. In *CHI*. ACM, 2015.
- [7] J. Ahmadi-Shokouh, S. Noghianian, E. Hossain, M. Ostadrahimi, and J. Dietrich. Reflection coefficient measurement for house flooring materials at 57-64 GHz. In *IEEE GLOBECOM 2009*.
- [8] S. Bakhtiari, T. Elmer, N. Cox, N. Gopalsami, A. Raptis, S. Liao, I. Mikhelson, and A. Sahakian. Compact Millimeter-Wave Sensor for Remote Monitoring of Vital Signs. *Instrumentation and Measurement, IEEE Transactions on*, 61(3):830–841, March 2012.
- [9] H.-R. Chuang, H.-C. Kuo, F.-L. Lin, T.-H. Huang, C.-S. Kuo, and Y.-W. Ou. 60-GHz millimeter-wave life detection system (MLDS) for noncontact human vital-signal monitoring. *Sensors Journal, IEEE*, 12(3):602–609, 2012.
- [10] S. Gabriel, R. Lau, and C. Gabriel. The dielectric properties of biological tissues: II. Measurements in the frequency range 10 Hz to 20 GHz. *Physics in medicine and biology*, 1996.
- [11] O. P. Gandhi and A. Riazi. Absorption of millimeter waves by human beings and its biological implications. *Microwave Theory and Techniques, IEEE Transactions on*, 1986.
- [12] W. F. Ganong and K. E. Barrett. *Review of medical physiology*, volume 21. McGraw-Hill Medical eNew York New York, 2005.
- [13] Gurin. Finger Pulse Oximeters. <http://gurinproducts.com/products/oximeters/>.
- [14] H. Hwang, J. Yim, J.-W. Cho, C. Cheon, and Y. Kwon. 110 GHz broadband measurement of permittivity on human epidermis using 1 mm coaxial probe. In *Microwave Symposium Digest, 2003*. IEEE.
- [15] IEEE P802.11adTM/D4.0. Part 11: Wireless LAN Medium Access Control (MAC) and Physical Layer (PHY) Specifications Amendment 3: Enhancements for Very High Throughput in 60 GHz. *IEEE Computer Society*.
- [16] T.-Y. J. Kao and J. Lin. Vital sign detection using 60-GHz Doppler radar system. In *Wireless Symposium (IWS), 2013 IEEE International*, pages 1–4. IEEE, 2013.
- [17] B. Langen, G. Lober, and W. Herzig. Reflection and transmission behaviour of building materials at 60 GHz. In *PIMRC*. IEEE, 1994.
- [18] J. Liu, Y. Wang, Y. Chen, J. Yang, X. Chen, and J. Cheng. Tracking Vital Signs During Sleep Leveraging Off-the-shelf WiFi. In *MobiHoc '15*.
- [19] I. V. Mikhelson, P. Lee, S. Bakhtiari, T. W. Elmer, A. K. Katsaggelos, and A. V. Sahakian. Noncontact millimeter-wave real-time detection and tracking of heart rate on an ambulatory subject. *Information Technology in Biomedicine, IEEE Transactions on*, 2012.
- [20] T. Nitsche, A. B. Flores, E. W. Knightly, and J. Widmer. Steering with Eyes Closed: mm-Wave Beam Steering without In-Band Measurement. In *IEEE INFOCOM 2015*.
- [21] Pasternack. Pasternack. <http://www.pasternack.com/60-ghz-test-development-system-pem003-kit-p.aspx>.
- [22] N. Patwari, L. Brewer, Q. Tate, O. Kaltiokallio, and M. Bocca. Breathfinding: A Wireless Network That Monitors and Locates Breathing in a Home. *Selected Topics in Signal Proc., IEEE Journal of*, 2014.
- [23] D. T. Petkie, C. Benton, and E. Bryan. Millimeter-wave radar for vital signs sensing. International Society for Optics and Photonics, 2009.
- [24] R. Ravichandran, E. Saba11, K.-Y. Chen, M. Goel, S. Gupta, and S. N. Patel. WiBreathe: Estimating Respiration Rate Using Wireless Signals in Natural Settings in the Home. In *Percom*. IEEE, 2015.
- [25] S. Sur, V. Venkateswaran, X. Zhang, and P. Ramanathan. 60 GHz Indoor Networking through Flexible Beams: A Link-Level Profiling. In *Sigmetrics '15*. ACM.
- [26] E. M. Tapia. *Using machine learning for real-time activity recognition and estimation of energy expenditure*. PhD thesis, MIT, 2008.
- [27] T. Wei and X. Zhang. mTrack: High-Precision Passive Tracking Using Millimeter Wave Radios. In *MobiCom '15*, New York, NY, USA. ACM.
- [28] Z. Yang, P. H. Pathak, Y. Zeng, and P. Mohapatra. Sensor-assisted codebook-based beamforming for mobility management in 60 ghz wlans. In *Mobile Ad Hoc and Sensor Systems (MASS), 2015 IEEE 12th International Conference on*, pages 333–341, Oct 2015.
- [29] Y. Zeng, P. H. Pathak, Z. Yang, and P. Mohapatra. Human tracking and activity monitoring using 60 ghz mmwave. In *2016 15th ACM/IEEE International Conference on Information Processing in Sensor Networks (IPSN)*, pages 1–2. IEEE, 2016.
- [30] M. Zhadobov, N. Chahat, R. Sauleau, C. Le Quement, and Y. Le Drean. Millimeter-wave interactions with the human body: state of knowledge and recent advances. *Inter. Journal of Microwave Technologies*, 2011.
- [31] X. Zhou, Z. Zhang, Y. Zhu, Y. Li, S. Kumar, A. Vahdat, B. Y. Zhao, and H. Zheng. Mirror Mirror on the Ceiling: Flexible Wireless Links for Data Centers. In *ACM SIGCOMM '12*.
- [32] Y. Zhu, Z. Zhang, Z. Marzi, C. Nelson, U. Madhow, B. Zhao, and H. Zheng. Demystifying 60GHz Outdoor Picocells. In *MobiCom '14*.